Anomalous Polymer Sedimentation Far from Equilibrium

Xaver Schlagberger and Roland R. Netz

Physics Department, Technical University Munich, 85748 Garching, Germany
(Received 20 September 2006; published 20 March 2007)

A single flexible polymer in strong sedimentation fields is investigated using hydrodynamic simulations and scaling arguments. For short chains and small fields compaction is observed. For elevated fields or long chains the chain stretches and the sedimentation coefficient decreases, in agreement with ultracentrifuge experiments on linear as well as circular DNA. For very large fields a tadpole forms consisting of a compact leading head and a trailing stretched tail.

Analytical ultracentrifugation has become a widespread tool for the characterization and separation of biomolecules [1,2]. In a sedimentation velocity experiment the moving boundary of the investigated substance with time is recorded to obtain the sedimentation coefficient S (defined as the radial velocity divided by the centrifugal force) [1]. In a sufficiently dilute solution, interactions between macromolecules are negligible, such that mass and conformation alone determine S. Early on, it has been shown that dilute solutions of long DNA ($>10^8$ Da $\approx 10^5$ base pairs) exhibit a decrease of S with increasing rotor speed [3,4]. This sedimentation anomaly can be explained by inhomogeneous friction in the chain [5,6]: The coil interior is hydrodynamically shielded while the chain ends, which on average are located at the coil exterior, receive more drag; consequently, the chain ends lag behind, the coil is stretched, the hydrodynamic radius increases, and the sedimentation coefficient goes down. Zimm's theory correctly predicts the functional dependence of S on rotor speed and molecular mass, but the spectacular quantitative agreement between theory and experiments [5] was later claimed to be due to a glitch in the calculations [4]. More seriously, Zimm's preaveraging approximation (PAA) predicts a null effect for polymer rings, in contrast to experiments on DNA loops [7].

In this Letter we use hydrodynamic simulations to study linear and circular sedimenting polymers. For short self-avoiding chains, compaction is caused by hydrodynamic chain recirculation. For longer chains and increasing sedimentation fields the chain elongates and consists of a compact (leading) part and a stretched (trailing) part, resembling a tadpole for very large fields. The observed behavior is similar for linear and circular polymers, in agreement with experiments. Scaling descriptions for chain radius and mobility are presented and compare favorably with simulations and experiments. By implementing Zimm's PAA in the simulations we can recover his results; interestingly, we find the hydrodynamic PAA to be a less serious approximation than the neglect of self-avoidance.

Modeling the polymer by N spheres, the velocity of the ith monomer follows from the Langevin equation as

$$\dot{\mathbf{r}}_i(t) = \sum_{j=1}^{N} \boldsymbol{\mu}_{ij} \cdot [-\nabla_{\mathbf{r}_j} U(\{\mathbf{r}_k\}) + G\hat{e}_z] + \boldsymbol{\xi}_i(t), \quad (1)$$

where G is a constant sedimentation force in the z direction acting on each monomer, and $\boldsymbol{\xi}_i$ a vectorial Gaussian random force with zero mean providing coupling to a heat bath and correlated according to the fluctuation-dissipation theorem as $\langle \boldsymbol{\xi}_i(t) \otimes \boldsymbol{\xi}_j(t') \rangle = 2k_BT\delta(t - t')\boldsymbol{\mu}_{ij}$. Hydrodynamic interactions between monomers i and j are included via the mobility tensor $\boldsymbol{\mu}_{ij}$. In most simulations we use the position-dependent Rotne-Prager tensor [8]; as a test we perform some simulations using Zimm's PAA given by $\boldsymbol{\mu}_{ij} = (6\pi^3|i - j|)^{-1/2}\mathbf{I}/(2\eta a)$ [9]. The mobility self-part is given by the Stokes mobility of a sphere with radius a, $\boldsymbol{\mu}_{ii} = \mathbf{I}/(6\pi\eta a) \equiv \mathbf{I}\mu_0$, where $\mathbf{I}$ is the 3×3 unit matrix and η the solvent viscosity (water). The inter-action potential U is in most simulations

$$U(\{\mathbf{r}_k\}) = \epsilon_{LJ}\sum_{i<j}\Theta(2a - r_{ij})\left[\frac{(2a)^{12}}{r_{ij}^{12}} - \frac{2(2a)^6}{r_{ij}^6} + 1\right]$$
$$+ \sum_{i=1}^{N-1}\frac{\gamma}{4a}[r_{ii+1} - 2a]^2, \quad (2)$$

and it consists of a truncated Lennard-Jones potential to account for chain self-avoidance and springs between nearest neighbors. $\Theta(x)$ is the Heaviside step function, and $r_{ij} = |\mathbf{r}_i - \mathbf{r}_j|$. Choosing a stretching modulus $\gamma \geq 400G$ is sufficient to approximate the freely-jointed chain model (FJC) with essentially constant bond length. For a self-avoiding (SA) chain, the repulsive potential strength is chosen as $\epsilon_{LJ} = k_BT$, for an ideal chain $\epsilon_{LJ} = 0$. For a Gaussian chain, the second line in Eq. (2) is replaced by $\sum \gamma r_{ii+1}^2/(4a)$ with a harmonic spring stiffness $\gamma = 3k_BT/(2a)$ which gives an equilibrium mean-squared bond length of $2a$.

For simulations, Eq. (1) is discretized with a time step Δ and all variables are rescaled by a and k_BT as $\tilde{\gamma} = \gamma a/k_BT$, $\tilde{G} = Ga/k_BT$, and $\tilde{\Delta} = \Delta\mu_0 k_BT/a^2$. Depending on chain length and field strength, we choose $\tilde{\Delta}$ between 3×10^{-5} and 0.005. In the simulations (consisting of up to 10^8 steps) the chain is first equilibrated with a slowly
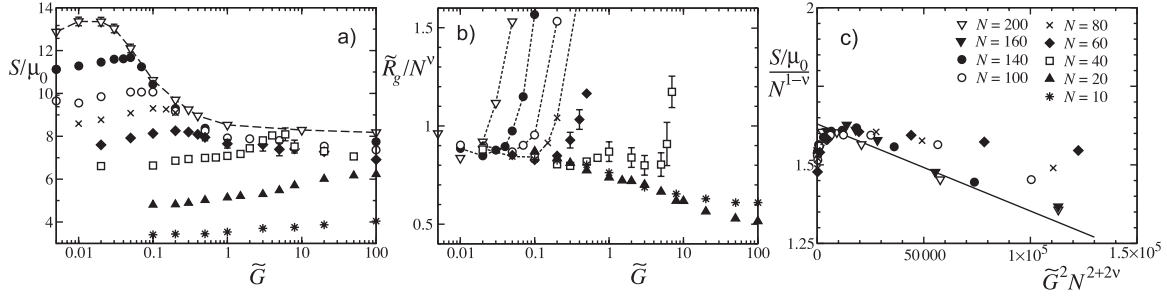
FIG. 1.   (a) Sedimentation coefficient S/μ_0 of a self-avoiding linear FJC for several monomer numbers N as a function of sedimenting field $\tilde{G} = Ga/k_BT$. The $N = 200$ results (broken line) give an upper envelope. (b) Reduced radius of gyration R_g/aN^ν for the same parameters using $\nu = 3/5$, showing an initial chain compaction and (for larger G) a chain stretching. (c) Scaling plot of the low-field data from (a); the solid line is given by $SN^{\nu-1}/\mu_0 = 1.63 - 2.77 \times 10^{-6}\tilde{G}^2N^{2+2\nu}$.

increasing field before averages are taken. Errors are calculated using block averaging and only shown if larger than the symbol size. The sedimentation coefficient is $S = \sum_i \langle \dot{\mathbf{r}}_i \rangle / (NG)$ and depends strongly on the chain conformation if hydrodynamics are properly included.

We first discuss a linear SA FJC with full hydrodynamic interactions (HI). Figure 1(a) shows S/μ_0 over four decades of $\tilde{G}$ for chains with $N = 10$ to $N = 200$ monomers. Except for the two shortest chains, S is nonmonotonic: For small fields S increases slightly, which is caused by a chain compaction. This is demonstrated in Fig. 1(b) where the rescaled radius of gyration R_g/aN^ν, defined as $R_g = (\sum_i \langle (\mathbf{r}_i - \mathbf{R}_M)^2 \rangle / N)^{1/2}$ (where $\mathbf{R}_M = \sum_i \mathbf{r}_i/N$ is the center of mass) exhibits a slight decrease for small $\tilde{G}$ (in equilibrium, one expects $R_g \sim N^\nu$ with $\nu = 3/5$ [9]). After passing through a maximum S drops considerably until it saturates at a much lower value than for the unperturbed ($G \rightarrow 0$) chain. This is paralleled by a sharp increase in R_g, which defines a critical field $\tilde{G}^\star$ at which a chain starts to unfold. Interestingly, the curve S for the longest chain ($N = 200$) forms an upper envelope for the other chain lengths, i.e., longer means faster. The progressive chain stretching as $\tilde{G}$ or N grows is visualized by snapshots in Fig. 2.

We now present a blob argument for the *compaction* of a sedimenting chain. In the nondraining regime, a chain of radius R sediments with a velocity given by Stokes' law $v \sim \mu_0GNa/R$ [9]. The hydrodynamic drag acts primarily on peripheral chain segments, inducing vortexlike monomer recirculation similar to the flow pattern in a smoke ring. We assume the typical internal velocity to scale as v, like the overall coil sedimentation speed. We partition the chain into blobs consisting of g monomers and unperturbed size $\xi \sim ag^\nu$. The assumption of equilibrium scaling inside blobs holds as long as the recirculation time $\tau_V \sim \xi/v$ is larger than the blob relaxation time τ_R, the blob size thus follows from $\tau_R \sim \tau_V$. Neglecting entanglement effects, one has $\tau_R \sim \xi^3/(a\mu_0k_BT)$, which leads to $\xi^2 \sim k_BTR/(GN)$. Beyond the blob size, the chain cannot relax and is condensed by the recirculation shear, suggesting compact scaling $R \sim \xi(N/g)^{1/3}$. Putting everything to-

gether, the chain radius scales as $R/a \sim N^\alpha\tilde{G}^\delta$ with $\alpha = (1-\nu)/(3\nu+1)$ and $\delta = (1-3\nu)/(3\nu+1)$. For small fields $\tilde{G} < \tilde{G}^{\text{com}} \sim N^{-1-\nu}$, the blob size is larger than the chain radius, $g > N$, and the chain conformation is unperturbed by sedimentation; for larger fields $\tilde{G} > \tilde{G}^{\text{com}}$ compaction is predicted. From the simulation results for S and R_g in Fig. 1 slight compaction is seen for short chains and small fields only; otherwise, the overall chain size is dominated by the stretched tail and compaction is limited to the head region.

We now discuss the mechanism for *stretching* and start with the *strong-stretching regime* (i.e., very large driving field G). As seen from the simulation snap shot for $\tilde{G} = 1$ in Fig. 2(a), the chain adopts a "tadpole" configuration consisting of a compact head of N_h monomers followed by a straight tail of $N_t = N - N_h$ monomers (similar to conformations observed when a collapsed chain is stretched by an external force acting on one end only [10]). From the tail stretching it follows that the head pulls the tail with some force F_s, which incidentally also orients the tadpole. Neglecting hydrodynamic interactions between head and tail (which contribute higher-order corrections), the head
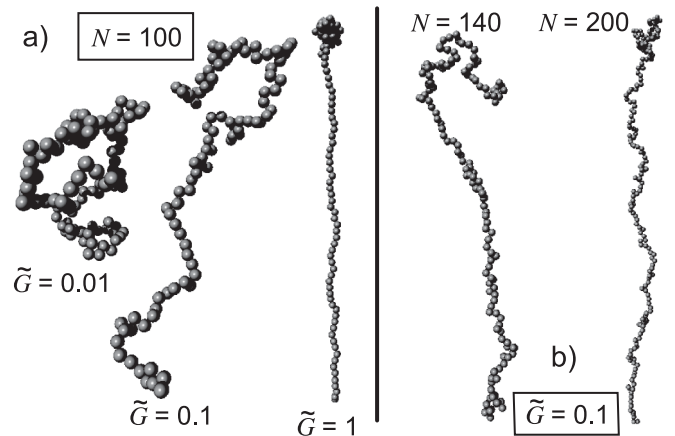
FIG. 2.   (a) Typical chain configurations for $N = 100$ at different force strengths. The force points upwards. (b) Simulation snapshots at $\tilde{G} = 0.1$ for $N = 140$ and 200.

velocity is $v_h \sim (GN_h - F_s)\mu_0 a/R_h \sim (GN_h - F_s)N_h^{-\nu}\mu_0$. Using the mobility of a straight cylinder (i.e., the tail is *strongly stretched*), the tail velocity is $v_t \sim (GN_t + F_s)\mu_0(\ln N_t - 1/2)/N_t$ [9]. The stretching force F_s is (in the absence of attractive monomer-monomer interactions) solely produced by internal friction in the recirculating head. Since it maximally scales as $F_s \sim GN_h$, it can be neglected in the above velocity expressions. In the stationary state head and tail velocities are equal, $v_h \sim v_t$, leading to a logarithmically small head size $N_h \sim (\ln N)^{1/(1-\nu)}$ and a sedimentation velocity of

$$S/\mu_0 \sim v/G\mu_0 \sim (3/2)\ln N. \qquad (3)$$

The hydrodynamic stability of this tadpole configuration follows by considering small perturbations: assuming the tadpole to be oriented with the head in front and a trailing tail, a head that is slightly smaller than in the stationary state will slow down and push against the tail and thus grow back to its equilibrium size (and conversely). To directly test the large-field result, Eq. (3), we perform zero-temperature simulations for the SA FJC where the noise term ξ_i in Eq. (1) is omitted, choosing rescaled parameters $\gamma = 200G$ and $\epsilon_{LJ} = Ga$. The resulting sedimentation coefficients are shown in Fig. 3(a) (circles) and compare very well with the asymptotic result Eq. (3) (solid line). The numerical results for finite temperature, taken from Fig. 1(a) for constant $G = 100k_BT/a$ (triangles), approach the scaling law for $N \to \infty$.

Experimentally most relevant is the *weak-stretching regime* (small G). Here the boundary between head and tail is diffuse [see the snapshot for $N = 100$ and $\tilde{G} = 0.1$ in Fig. 2(a)] and the tail is slightly perturbed into an ellipsoid with short axes R_t and long axis L_t. As before, we equilibrate the head velocity $v_h \sim GN_h\mu_0 aR_h^{-1} \sim GN_h^{1-\nu}\mu_0$ with the tail velocity $v_t \sim GN_t\mu_0 aR_t^{-1}/(1 + L_t/4R_t)$ for which the mobility of an ellipsoid along its long axis is used [11]. For small force F_s the tail stretching is har-

monic, $L_t/R_t - 1 \sim (F_sR_t/kT)^2$. Assuming a stretching force $F_s \sim N_hG$ (meaning that all monomers in the head contribute via internal friction to F_s), a tail size of $R_t \sim N_t^\nu$, and requiring that $v_h \sim v_t$, we obtain in the small-G (*weak-stretching*) limit $N/2 - N_h \sim N^{3+2\nu}\tilde{G}^2$ and thus

$$S/\mu_0 = v/\mu_0 G \simeq c_1 N^{1-\nu} - c_2 N^{3+\nu}\tilde{G}^2. \qquad (4)$$

The N dependence of the correction factor is (with $\nu = 0.6$) in accord with experiments, where a scaling proportional to $N^{3.65}G^2$ is observed [3], and for the longest chains also in satisfactory agreement with an asymptotic fit to the simulation data in Fig. 1(c), which determines the coefficients as $c_1 = 1.63$ and $c_2 = 2.77 \times 10^{-6}$. This lends credibility to our scaling assumption $F_s \sim GN_h$.

In the *intermediate stretching regime*, $1/L_t < F_s/k_BT < 1/a$, the tail is stretched but not fully extended, i.e., $L_t \sim N_t F_s^{1/\nu-1}$ [12]. Using the scaling assumption $F_s \sim GN_h$ and the results for N_h in the strong and weak-stretching regimes, this translates into a sedimentation field range $\tilde{G}^{\star\star} < \tilde{G} < \tilde{G}^{\star\star\star}$ with $\tilde{G}^{\star\star} \sim N^{-1-\nu}$ and $\tilde{G}^{\star\star\star} \sim (\ln N)^{1/(\nu-1)}$. A modified scaling calculation yields a sedimentation coefficient $S/\mu_0 \sim \tilde{G}^{(\nu-1)/(\nu+1)}(\ln N)^{\nu/(\nu+1)}$ in good agreement with simulations [13], which complements the results in Eqs. (3) and (4). The actual onset of chain unfolding, which is determined from the maximum in S or the minimum in R_g, is shown in Fig. 3(b) and follows in the restricted available data range a scaling with $\tilde{G}^\star \sim N^{-2}$, at odds with the simulation observation that slight compaction sets in before chains stretch, i.e. $\tilde{G}^{\text{com}} < \tilde{G}^\star$. This conflict can be resolved by assuming that the threshold for compaction $\tilde{G}^{\text{com}}$ is lower than suggested by our scaling result $\tilde{G}^{\text{com}} \sim N^{-1-\nu}$ (which is plausible since it neglects entanglement effects) or that $\tilde{G}^\star$ scales differently so that a range $\tilde{G}^{\text{com}} < \tilde{G} < \tilde{G}^\star$ with compact chains exists. Alternatively, compaction of the chain as a whole could be observable only for short chains and always preempted by chain unfolding for long chains (as suggested by DNA sedimentation experiments). Experiments with long chains at weak sedimenting fields could clarify this issue. Note that local compaction in the head region is suggested by the scaling results and in fact seen in the simulations. Tadpole orientation and conformational stability require the torque $M \sim F_sL_t$ to be larger than k_BT. From $F_s \sim GN_h$, $L_t \sim N_t^\nu$, and $N_t \sim N_h \sim N$ this is equivalent to $\tilde{G} > \tilde{G}^{\star\star} \sim N^{-1-\nu}$ and coincides with the crossover between weak and intermediate stretching.

To estimate the importance of hydrodynamics, we also perform simulations using the PAA; since the velocity then is independent of the conformation, we calculate the sedimentation coefficient using the hydrodynamic tensor as $\bar{S}/\mu_0 = 3a\sum_{ij}\langle 1/r_{ij} + z_{ij}^2/r_{ij}^3\rangle/(4N)$, where the brackets represent the configurational average at finite field [5]. In Fig. 4(a) we compare $\bar{S}/\mu_0$ for three cases: ideal Gaussian (circles), self-avoiding Gaussian (squares), and self-avoiding FJC (triangles), each for both full hydrodynamics
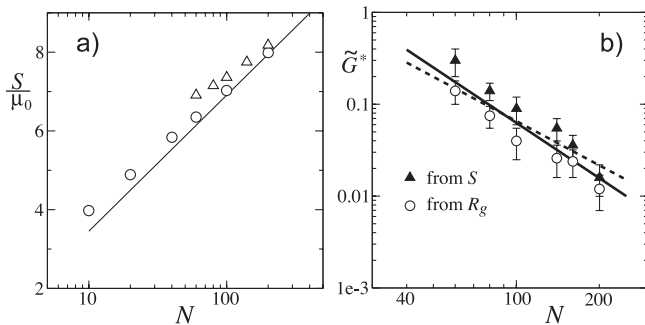
FIG. 3. (a) Zero (circles) and finite-temperature simulations ($Ga = 100k_BT$, triangles) compared with the asymptotic scaling law Eq. (3) $S/\mu_0 \sim (3/2)\ln N$ (solid line). (b) Unfolding field strength $\tilde{G}^\star$, defined graphically in Fig. 1(a) and 1(b) from the maximum of S (triangles) and the minimum of R_g (circles). The solid line is a heuristic fit with $\tilde{G}^\star = 670N^{-2}$, the broken line denotes $\tilde{G}^\star \sim N^{-1-\nu}$.
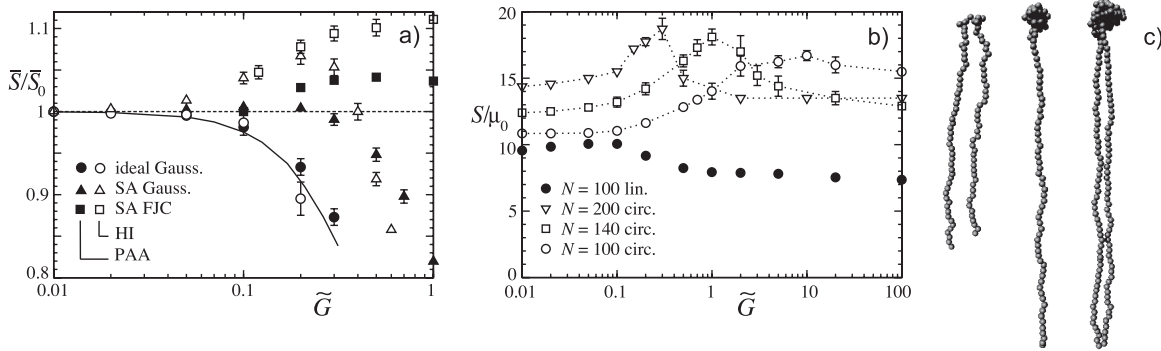
FIG. 4.   (a) Relative approximate sedimentation coefficient $\bar{S}/\bar{S}_0$ for a linear $N = 40$ chain modeled as a SA FJC (squares), SA Gaussian (triangles) and ideal Gaussian chain (circles). Open symbols include full hydrodynamics (HI), filled ones use preaveraging (PAA). The solid line is Zimm's PAA calculation for an ideal Gaussian chain [5]. (b) Sedimentation coefficient of *circular* (open symbols) and *linear* chains (closed symbols), all for SA FJC with full HI. (c) Snapshots, from left to right: $N = 100$ linear SA FJC with PAA, same chain with full HI, and $N = 200$ circular SA FJC with full HI, all at $\tilde{G} = 1$.

(HI, open symbols) and PAA (filled symbols), for a chain length $N = 40$ and divided by the zero-field limit $\bar{S}_0 = \bar{S}(G \to 0)$. Zimm's PAA calculation at small fields for an ideal Gaussian chain [5] is included (solid line) and describes quantitatively both the HI and PAA simulations of an ideal Gaussian chain (circles). Surprisingly, self-avoidance effects drastically change the simulation results, even if preaveraging is used. The conclusion is that self-avoidance is an important effect for strongly sedimenting chains. Interestingly, the conformations obtained within PAA are wrong even when a SA-FJC model is used, as demonstrated in Fig. 4(c), where a snapshot shows a configuration where both tails are trailing and the symmetry breaking between the two tails is not obtained.

The preaveraging approach yields no sedimentation anomaly for circular chains [5,7]. Experimentally, on the other hand, *circular* DNA exhibits a sedimentation constant dependence similar to linear DNA with half the length [7], which is relevant in the context of DNA supercoiling [14]. In Fig. 4(b) we compare S/μ_0 for circular chains of different lengths with the result for a linear chain with $N = 100$ (filled circles). The circular $N = 200$ chain shows the onset of unfolding at a similar force as the linear $N = 100$ chain. This becomes clear when looking at snapshots at driving force $\tilde{G} = 1$ in Fig. 4(c): The circular chain with $N = 200$ (to the right) forms a tadpole similar in size and shape to the linear $N = 100$ chain (in the middle) except that the tail is double stranded, which explains the experimental finding.

To get a feel for the experimental relevance, we consider a 180 kbp DNA strand in a centrifuge with radius $x = 0.05$ m spinning at $60\omega/2\pi = 50\,000$ rpm [4]. For an effective monomer with radius $a = 1$ nm, corresponding mass m_0 of six base pairs, and a buoyancy correction factor of $1 - \rho_w/\rho_{DNA} = 0.436$, where ρ_w and ρ_{DNA} are the densities of water and DNA, we obtain a rescaled field of $\tilde{G} = m_0(1 - \rho_w/\rho_{DNA})x\omega^2 a/k_B T \sim 10^{-6}$, similar to the theoretically predicted critical unfolding field given by $\tilde{G}^\star \sim 10^{-6}$ [using $N = 30\,000$ and $\tilde{G}^\star = 670N^{-2}$, see

Fig. 3(b)]. Indeed, the onset of chain unfolding is obtained in typical ultracentrifuge experiments. A quantitative prediction of the DNA sedimentation anomaly [4], however, is at present not feasible, since the nonuniversal dependence on the ratio of chain diameter and persistence length is not included. A more direct comparison might be possible with flexible synthetic chains, where this complication is absent. The hydrodynamic compaction predicted here for short chains might have been observed with certain proteins that undergo conformational changes under sedimentation [15].

[1] *Analytical Ultracentrifugation in Biochemistry and Polymer Science*, edited by S. E. Harding *et al.* (Royal Soc. Chem., Cambridge, 1993).

[2] T. Laue and W. F. Stafford, Annu. Rev. Biophys. Biomol. Struct. **28,** 75 (1999).

[3] I. Rubenstein and S. B. Leighton, Biophys. Chem. **1,** 292 (1974).

[4] R. Clark and C. Lange, Biopolymers **19,** 945 (1980).

[5] B. H. Zimm, Biophys. Chem. **1,** 279 (1974).

[6] D. Ertas and M. Kardar, Phys. Rev. E **48,** 1228 (1993).

[7] E. J. Ralston and V. N. Schumaker, Biophys. Chem. **9,** 375 (1979).

[8] D. L. Ermak and J. A. McCammon, J. Chem. Phys. **69,** 1352 (1978).

[9] M. Doi and S. F. Edwards, *The Theory of Polymer Dynamics* (Clarendon, Oxford, 1986).

[10] I. R. Cooke and D. R. M. Williams, Europhys. Lett. **64,** 267 (2003).

[11] J. Happel and H. Brenner, *Low Reynolds Number Hydrodynamics* (Kluwer, The Hague, 1983).

[12] P. Pincus, Macromolecules **9,** 386 (1976).

[13] X. Schlagberger and R. R. Netz (to be published).

[14] T. Odijk, Colloids Surf. A **210,** 191 (2002).

[15] J. C. Borges *et al.*, J. Biol. Chem. **280,** 13 671 (2005).